Identifiability and Parameter Estimation of the Single Particle Lithium-Ion Battery Model

Adrien M. Bizeray ⓘ, Jin–Ho Kim, Stephen R. Duncan, *Member, IEEE*,
and David A. Howey ⓘ, *Senior Member, IEEE*

Abstract—This paper investigates the identifiability and estimation of the parameters of the single particle model (SPM) for lithium-ion battery simulation. Identifiability is addressed both in principle and in practice. The approach begins by grouping parameters and partially nondimensionalising the SPM to determine the maximum expected degrees of freedom in the problem. We discover that excluding open-circuit voltage (OCV), there are only six independent parameters. We then examine the structural identifiability by considering whether the transfer function of the linearized SPM is unique. It is found that the model is unique provided that the electrode OCV functions have a known nonzero gradient, the parameters are ordered, and the electrode kinetics are lumped into a single charge-transfer resistance parameter. We then demonstrate the practical estimation of model parameters from measured frequency-domain experimental electrochemical impedance spectroscopy data, and show additionally that the parametrized model provides good predictive capabilities in the time domain, exhibiting a maximum voltage error of 20 mV between the model and the experiment over a 10-min dynamic discharge.

Index Terms—Batteries, modeling, parameter estimation, system identification.

Nomenclature

A. Roman

$\mathcal{A}$	Electrode surface area, m^2.
a_i	Specific active surface area, m^{-1}.
c_e	Electrolyte lithium concentration, $mol \cdot m^{-3}$.
c_i	Lithium concentration (active material), $mol \cdot m^{-3}$.
c_i^0	Initial lithium concentration, $mol \cdot m^{-3}$.
c_i^{max}	Maximum lithium concentration, $mol \cdot m^{-3}$.
c_i^s	Surface lithium concentration, $mol \cdot m^{-3}$.
D_i	Electrode active material diffusivity, $m^2 \cdot s^{-1}$.
$\mathcal{F}$	Faraday's constant, $C \cdot mol^{-1}$.
H^0	SPM transfer function, Ω.
H_i^d	Diffusion model transfer function, A^{-1}.
I	Applied current, A.
$i_{0,i}$	Exchange current density, $A \cdot m^{-2}$.
j_i	Reaction rate, $mol \cdot m^{-2} \cdot s^{-1}$.
k_i	Reaction rate constant, $m^{2.5} \cdot mol^{-0.5} \cdot s^{-1}$.
L_j	Single DoD loss function, Ω^2.
L	Combined DoDs loss function, Ω^2.
N_ω	Number of data points per EIS measurement.
N_{DoD}	Number of EIS data sets at different DoDs.
Q	Charge/discharge capacity, C.
Q_i^{th}	Theoretical electrode capacity, C.
R	Gas constant, $J \cdot mol^{-1} \cdot K^{-1}$.
R_{ct}^0	Charge-transfer resistance, Ω.
R_i	Active material particle radius, m.
r_i	Particle radial coordinates, m.
$\bar{r}$	Particle dimensionless radial coordinates.
T	Temperature, K.
t	Time, s
U_i	Open-circuit voltage, V.
$\bar{u}_i$	Change of variable $\bar{r}\bar{x}_i$.
V	Cell terminal voltage, V.
$\bar{V}^0$	Voltage deviation from equilibrium, V.
V_i	Volume of electrode active material, m^3.
x_0	Linearization reference point.
x_i	Lithium stoichiometry (active material).
$\mathbf{x}_i^0$	Initial lithium stoichiometry.
x_i^s	Surface lithium stoichiometry.
$\bar{x}_i$	Change of variable $x_i - x_i^0$.
Z_j	Measured cell impedance, Ω.

B. Greek

α_i	Anodic charge transfer coefficient.
α_i^0	OCV gradient with respect to stoichiometry, V.
β_i^0	OCV gradient with respect to capacity, $V/(A \cdot s)$.
δ_i	Electrode thickness, m.
ϵ_i	Solid-phase volume fraction.
η_i	Overpotential, V.
θ_j	Grouped parameter.
$\boldsymbol{\theta}$	Vector of grouped parameters, $\boldsymbol{\theta} \in \mathbb{R}^6$.
$\tilde{\boldsymbol{\theta}}$	Vector of identifiable parameters, $\tilde{\boldsymbol{\theta}} \in \mathbb{R}^3$.
$\boldsymbol{\theta}_{id}$	Vector of identified parameters.
τ_i^d	Diffusion time constant, s.
τ_i^k	Kinetic time constant, s.
ω	Angular frequency, $rad \cdot s^{-1}$.

I. INTRODUCTION

IN ADDITION to their widespread use in consumer electronics, the importance of lithium-ion batteries is increasing in large-scale energy storage applications, such as automotive, off-grid and grid applications. Such large-scale battery energy storage systems are required to operate for a decade or more. Battery degradation that results in capacity and power fade over time becomes a particularly important issue in applications with such long service life. However, battery-management system (BMS) technologies, currently used in commercial applications for monitoring and controlling batteries to ensure their safety, have very limited insights into battery degradation.

Two important functions of a conventional BMS are: 1) to monitor the battery voltage, current, and temperature and ensure that these remain within their region of safe operation and 2) to estimate unmeasurable metrics such as state of charge (SoC) and state of health (SoH). The SoC denotes the remaining energy in the cell compared to a fully charged cell, while the SoH is usually defined as the capacity or resistance of an aged cell compared to that of a pristine cell. A mathematical model of a battery is required to infer SoC and SoH from the available measurements of voltage, current, and temperature. Conventional BMSs commonly employ electrical equivalent circuit models (ECMs) consisting of a voltage source and a network of resistors and capacitors whose current–voltage response mimics that of a battery. The parameters of such ECMs may vary with SoC, SoH, current, and temperature and must, therefore, be identified from experimental data under a large range of operating conditions. However, the battery behavior predicted by ECMs cannot credibly be extrapolated outside the range of validity over which they have been parametrized. Also, accounting for battery degradation is challenging due to the lack of physical significance of the model parameters [1].

A. Motivations

In order to improve the lifetime performance of battery packs, researchers are investigating the application of physics-based electrochemical models instead of ECMs in the BMS, for example to enable electrochemical control of fast charging [2]–[4]. Due to their physical basis, such first-principle models can provide insights into battery aging because they can more easily be coupled to degradation models. Physics-based models could be solved online in next-generation BMSs to enable health-aware management and control algorithms that use internal electrochemical safety limits (e.g., local overpotential or lithium concentration) instead of the commonly employed terminal voltage and current safety limits [5], [6].

However, this is a challenging research area from both the modeling and numerical solution perspective, and also the application perspective. One key challenge is whether such models are observable and can be used reliably for state estimation. Recent promising results indicate that electrochemical models could indeed be used in this way [1], [7]–[13]. Another important prerequisite for the use of an electrochemical model in a BMS is that the model parameters are credible, not only to recreate the cell voltage response accurately, but so that

predictions of internal states, such as overpotential, are also accurate. In general, parameters in these models are obtained from the literature (for example [1], [14]), and whilst this is useful for initial design studies of cell performance, for use in a BMS, the model must be parametrized specifically for the cells used in the pack. Relatively few authors have tackled this parameter estimation problem [15]–[19] although it has been investigated in the context of ECMs of battery dynamics [20]–[23]. This paper is, therefore, motivated by the need to obtain meaningful model parameters for using an electrochemical battery models for control and estimation purposes.

B. Contributions

In this paper, we investigate the parameter estimation challenge in a simplified version of the "Doyle–Fuller–Newman" pseudo-2-D (P2-D) lithium-ion battery model [24], the so-called single particle model (SPM) [25], [26], first to see whether groups of parameters are identifiable in principle, and then to investigate whether in practice they can be identified from simulated and experimental frequency-domain electrochemical impedance spectroscopy (EIS) data [27].

The main contribution of our work is to show the importance of considering the structural and practical identifiability of model parameters before undertaking any parameter estimation. Attempting the identification of all model parameters simultaneously without considering their identifiability is likely to lead to ill-conditioned optimization problems. An electrochemical model identified in such a way may indeed fit the battery voltage and current response well, but the estimated parameters will have no physical significance, and therefore, the internal states cannot be reliably used for control. We also demonstrate the parameter estimation of an electrochemical battery model from frequency-domain data obtained from commercial cells, and this is a relatively new and unexplored research topic [28], [29].

Our first key result is that the parameter identifiability of any lithium-ion battery model, whether ECM or the first-principle electrochemical model, is largely conditional on the slope of each electrodes' open-circuit voltage (OCV) as a function of SoC. A flat OCV curve overshadows all dynamics and results in parameter unidentifiability. A second key message from this paper is that physics-based models for lithium-ion batteries are over-parametrized, and therefore, one must try to identify the minimum number of identifiable grouped parameters prior to attempting any parameter estimation.

II. SINGLE PARTICLE MODEL

The SPM was first introduced by Atlung *et al.* [25] and later extended to lithium-ion batteries by Ning *et al.* [26]. The SPM is an electrochemical battery model describing the cell thermodynamics, the diffusion of lithium in the active material of the electrodes, and the interfacial kinetics of the lithium intercalation/deintercalation reaction at the electrode/electrolyte interface. In contrast with the more complex P2-D model [24], electrolyte dynamics are neglected in the SPM, and therefore, the reaction rate is assumed uniform for

each electrode. We chose the SPM in this paper because it is the "simplest" electrochemical lithium-ion model and a good starting point for parameter identification studies. We anticipate that our methodology could be extended to other electrochemical models suitable for higher C-rates. Importantly, we do not anticipate that our main conclusions will change with respect to more complex models: the electrode OCV functions will remain as a key factor in paramaterization and the over-parametrization issue will become more challenging. Although the validity range of the SPM may vary depending on the physico-chemical properties of the cell (e.g., electrolyte conductivity and porosity), it is commonly accepted in the literature that the SPM is valid at currents below $1C$ to $2C$,[1] where concentration gradients in the electrolyte are negligible [5], [15], [30]. For many applications, including electric vehicles and grid storage, average C-rates are lower than $1C$ and this limitation is not particularly restrictive. In fact, we demonstrate later in this paper that reasonable voltage errors may be obtained with the *linearized* SPM on data including peaks in current of up to $6C$. Finally, for the purpose of parameter estimation, in our work we used frequency-domain linear response EIS experimental data. Linear EIS data are recorded by applying a small ac current signal (with zero dc offset) to the cell with an amplitude much lower than $1C$ (typically around $C/10$) to ensure that the cell voltage response remains linear. It is, therefore, reasonable to use the SPM for modeling the battery impedance from linear EIS data with such low amplitude currents.

A. Spherical Particle Diffusion Model

In the SPM, the diffusion of lithium in the active material of each battery electrode i (anode or cathode) is governed by the Fickian diffusion equation in spherical coordinates

$$\frac{\partial c_i}{\partial t} = \frac{D_i}{r_i^2} \frac{\partial}{\partial r_i} \left(r_i^2 \frac{\partial c_i}{\partial r_i} \right) \tag{1}$$

where r_i denotes the radial coordinates, c_i is the lithium concentration profile, and D_i is the lithium diffusion coefficient (assumed uniform and constant) in electrode i. The subscript i either takes the value $+$ or $-$ to refer to the cathode or anode domain, respectively. The diffusion equation is subject to Neumann boundary conditions at the particle center $r_i = 0$ and surface $r_i = R_i$

$$\left. \frac{\partial c_i}{\partial r_i} \right|_{r_i = 0} = 0 \quad \text{and} \quad D_i \left. \frac{\partial c_i}{\partial r_i} \right|_{r = R_i} = -j_i \tag{2}$$

and the initial condition equation

$$c_i(0, r_i) = c_i^0 \tag{3}$$

where c_i^0 is the initial concentration profile in each particle. The molar flux j_i in (2) expresses the rate of the lithium intercalation/deintercalation reaction. In contrast to the Doyle–Fuller–Newman model [24] where algebraic equations must be solved to obtain the molar flux for each particle, the molar

---

[1]In the battery literature, the electrical current is commonly expressed as a *C*-rate, which is a value of current normalized by the cell capacity so that a current amplitude of $1C$ will discharge the cell in 1 h.

fluxes in the SPM can be directly related to the applied battery current I through the relationships

$$j_- = \frac{+I}{a_- \delta_- \mathcal{F} \mathcal{A}} \quad \text{and} \quad j_+ = \frac{-I}{a_+ \delta_+ \mathcal{F} \mathcal{A}} \tag{4}$$

where $a_i = 3\epsilon_i / R_i$ is the specific active surface area in electrode i, ϵ_i is the volume fraction of active material in an electrode, $\mathcal{F}$ is the Faraday constant, $\mathcal{A}$ is the electrode surface area that is assumed equal for both electrodes, and δ_i is the thickness of the electrode i. By convention, the battery discharge current is positive and the charging current is negative. The anode is the negative electrode upon discharge and the cathode is the positive electrode. Although strictly speaking these swap upon charging, we will use the widely accepted abuse of terminology that the "anode" is the negative electrode and the "cathode" is the positive electrode in this paper. The above-mentioned molar flux expressions assume an electrochemical reaction involving a single electron transfer, which is the case for the lithium intercalation/deintercalation reaction.

B. Voltage Measurement Equation

The initial-boundary value problems (1)–(3) for each electrode constitute the dynamic part of the SPM. The battery terminal voltage V is given by the nonlinear measurement equation

$$V = U_+(x_+^s) - U_-(x_-^s) + \eta_+ - \eta_-. \tag{5}$$

The anode and cathode OCV U_- and U_+, respectively, are empirical nonlinear functions of the surface stoichiometry x_i^s of each particle defined according to

$$x_i^s = c_i^s / c_i^{\max}. \tag{6}$$

The overpotential η_i is the voltage drop due to the departure from equilibrium potential associated with the intercalation/deintercalation reaction in each electrode. The relationship between the reaction rate j_i and the overpotential η_i is given by the Butler–Volmer kinetics equation [24]

$$j_i = \frac{i_{0,i}}{\mathcal{F}} \left[\exp\left(\frac{\alpha_i \mathcal{F}}{RT} \eta_i \right) - \exp\left(\frac{-(1 - \alpha_i)\mathcal{F}}{RT} \eta_i \right) \right]. \tag{7}$$

The exchange current density $i_{0,i}$ depends on the reaction rate constant k_i and the reactants and products concentrations, i.e., the electrolyte concentration c_e (assumed constant in this model), and the lithium solid-phase concentration c_i^s at the surface of the particle, through the relation

$$i_{0,i} = k_i \mathcal{F} \sqrt{c_e} \sqrt{c_i^s} \sqrt{c_i^{\max} - c_i^s}. \tag{8}$$

By assuming that the anodic charge-transfer coefficients in (7) are $\alpha_i = 0.5$, i.e., anodic and cathodic charge-transfer coefficients are equal, the overpotential η_i can be expressed as a function of the reaction rate j_i as

$$\eta_i = \frac{2RT}{\mathcal{F}} \sinh^{-1} \left(\frac{j_i \mathcal{F}}{2 i_{0,i}} \right). \tag{9}$$

C. Identification of Grouped Parameters

First-principle models, such as the SPM, are usually over-parametrized in the sense that only a subset of parameters can be estimated from measured input–output data. A first necessary step toward credible parameter estimation is to reformulate the model in terms of the minimum number of parameter groups. In order to identify such groups of parameters, we first introduce the dimensionless radial coordinates $\bar{r} = r_i/R_i$, and the stoichiometry $x_i = c_i/c_i^{\max}$, instead of the concentration in the governing equations. In addition, the change of variable $\bar{x}_i = x_i - x_i^0$ is introduced, with $x_i^0 = c_i^0/c_i^{\max}$ being the initial stoichiometry in each particle, in order to set the initial condition to zero in the governing equations. Note that the time independent variable t is kept dimensional for simplicity because the diffusion time constants are different in each electrode. Introducing these dimensionless variables, the initial-boundary value problem (1)–(3) can be written as

$$\frac{\partial \bar{x}_i}{\partial t} = \frac{D_i}{R_i^2} \frac{1}{\bar{r}^2} \frac{\partial}{\partial \bar{r}} \left(\bar{r}^2 \frac{\partial \bar{x}_i}{\partial \bar{r}} \right) \tag{10}$$

subject to the boundary conditions

$$\left. \frac{\partial \bar{x}_i}{\partial \bar{r}} \right|_{\bar{r}=0} = 0 \quad \text{and} \quad \left. \frac{\partial \bar{x}_i}{\partial \bar{r}} \right|_{\bar{r}=1} = \frac{-R_i}{D_i c_i^{\max}} j_i \tag{11}$$

with initial conditions

$$\bar{x}_i(0, \bar{r}) = 0. \tag{12}$$

The boundary condition at the surface of the particle in each electrode can also be written in terms of the input current I instead of the fluxes j_i using relations (4) according to

$$\left. \frac{\partial \bar{x}_+}{\partial \bar{r}} \right|_{\bar{r}=1} = +\frac{R_+^2}{D_+} \frac{I}{3\epsilon_+ \delta_+ c_+^{\max} \mathcal{F} \mathcal{A}} \tag{13}$$

$$\left. \frac{\partial \bar{x}_-}{\partial \bar{r}} \right|_{\bar{r}=1} = -\frac{R_-^2}{D_-} \frac{I}{3\epsilon_- \delta_- c_-^{\max} \mathcal{F} \mathcal{A}}. \tag{14}$$

Similarly using relation (4), the expression for the overpotential in each electrode (9) becomes

$$\eta_+ = \frac{2RT}{\mathcal{F}} \sinh^{-1} \left(-\frac{R_+}{2k_+\sqrt{c_e}} \frac{1}{3\epsilon_+ \delta_+ c_+^{\max} \mathcal{F} \mathcal{A}} \frac{I}{\sqrt{x_+^s \left(1 - x_+^s \right)}} \right) \tag{15}$$

$$\eta_- = \frac{2RT}{\mathcal{F}} \sinh^{-1} \left(+\frac{R_-}{2k_-\sqrt{c_e}} \frac{1}{3\epsilon_- \delta_- c_-^{\max} \mathcal{F} \mathcal{A}} \frac{I}{\sqrt{x_-^s \left(1 - x_-^s \right)}} \right) \tag{16}$$

with the voltage measurement (5) expression unchanged. Six physically meaningful groups of parameters naturally arise in these equations. Indeed one can identify three groups of parameters for each electrode: a diffusion time constant τ_i^d, kinetics time constant τ_i^k, and the maximum theoretical electrode capacity Q_i^{th}. The expressions for these six physically meaningful groups of parameters are defined as follows:

$$\tau_+^d = \frac{R_+^2}{D_+} \quad \tau_-^d = \frac{R_-^2}{D_-} \tag{17}$$

$$\tau_+^k = \frac{R_+}{2\,k_+\sqrt{c_e}} \quad \tau_-^k = \frac{R_-}{2\,k_-\sqrt{c_e}} \tag{18}$$

$$Q_+^{\mathrm{th}} = -\epsilon_+ \delta_+ c_+^{\max} \mathcal{F} \mathcal{A} \quad Q_-^{\mathrm{th}} = +\epsilon_- \delta_- c_-^{\max} \mathcal{F} \mathcal{A}. \tag{19}$$

Note that for convenience the cathode theoretical capacity Q_+^{th} is defined negative by convention and without loss of generality, to yield the same model structure in both the anode and cathode. Substituting these grouped parameters into the governing equations results in the following diffusion equation for both the cathode and anode:

$$\frac{\partial \bar{x}_i}{\partial t} = \frac{1}{\tau_i^d} \frac{1}{\bar{r}^2} \frac{\partial}{\partial \bar{r}} \left(\bar{r}^2 \frac{\partial \bar{x}_i}{\partial \bar{r}} \right) \tag{20}$$

subject to the boundary conditions

$$\left. \frac{\partial \bar{x}_i}{\partial \bar{r}} \right|_{\bar{r}=0} = 0 \quad \text{and} \quad \left. \frac{\partial \bar{x}_i}{\partial \bar{r}} \right|_{\bar{r}=1} = -\frac{\tau_i^d}{3 Q_i^{\mathrm{th}}} I \tag{21}$$

with initial condition

$$\bar{x}_i(0, \bar{r}) = 0. \tag{22}$$

The voltage measurement equation remains

$$V = U_+\left(x_+^s\right) - U_-\left(x_-^s\right) + \eta_+ - \eta_- \tag{23}$$

with the cathode and anode overpotentials given as

$$\eta_+ = \frac{2RT}{F} \sinh^{-1} \left(\frac{\tau_+^k}{3 Q_+^{\mathrm{th}}} \frac{I}{\sqrt{x_+^s \left(1 - x_+^s \right)}} \right) \tag{24}$$

$$\eta_- = \frac{2RT}{F} \sinh^{-1} \left(\frac{\tau_-^k}{3 Q_-^{\mathrm{th}}} \frac{I}{\sqrt{x_-^s \left(1 - x_-^s \right)}} \right). \tag{25}$$

Inspecting (20)–(25), one can identify six groups of parameters θ_j that fully parametrize the SPM given by the parameter vector $\boldsymbol{\theta} \in \mathbb{R}^6$

$$\boldsymbol{\theta} = \left[\tau_+^d \quad \frac{\tau_+^d}{3 Q_+^{\mathrm{th}}} \quad \frac{\tau_+^k}{3 Q_+^{\mathrm{th}}} \quad \tau_-^d \quad \frac{\tau_-^d}{3 Q_-^{\mathrm{th}}} \quad \frac{\tau_-^k}{3 Q_-^{\mathrm{th}}} \right]^T. \tag{26}$$

Unlike the parameters defined in (17)–(19), these parameters θ_j appear only once and not as a product of each other in the model equations. Moreover, one can show that there is a one-to-one mapping between the six parameters θ_j and the six parameters (17)–(19) defined as

$$\begin{cases} \tau_+^d = \theta_1 \\ \tau_+^k = (\theta_1 \theta_3)/\theta_2 \\ Q_+^{\mathrm{th}} = \theta_1/(3\theta_2) \\ \tau_-^d = \theta_4 \\ \tau_-^k = (\theta_4 \theta_6)/\theta_5 \\ Q_-^{\mathrm{th}} = \theta_4/(3\theta_5). \end{cases} \tag{27}$$

Therefore, assuming that the initial electrode stoichiometries x_i^0 (i.e., SoC) are known and that the OCVs are known functions of the surface stoichiometry for each electrode, the six parameters contained in $\boldsymbol{\theta}$, or equivalently the six parameters defined in (17)–(19), are sufficient to fully parametrize the SPM.

III. Structural Identifiability

Six grouped parameters have been identified as sufficient to fully parametrize the SPM. However, this does not imply that these six parameters can be identified from the battery current–voltage response. Several approaches can be used to investigate the parameter identifiability of a dynamical model from input–output data. In this section, the so-called *structural identifiability* [31] of the SPM is discussed. Structural identifiability investigates the mathematical identifiability of the model irrespective of the identification data considered (which are also assumed noise free). A definition of structural identifiability for linear time-invariant dynamic models that can be cast into a transfer function $H(s, \theta)$ parametrized by a vector of parameters θ is given as follows [32], [33]:

Definition 1: Consider a model structure $\mathcal{M}$ with the transfer function $H(s, \theta)$ parametrized by $\theta \in \mathcal{D} \subset \mathbb{R}^n$ where n denotes the number of parameters of the model. The identifiability equation for $\mathcal{M}$ is given as

$$H(s, \theta) = H(s, \theta^*) \quad \text{for almost all } s \tag{28}$$

where $\theta, \theta^* \in \mathcal{D}$. The model structure $\mathcal{M}$ is said to be:

1) *Globally identifiable* if (28) has a unique solution in $\mathcal{D}$;
2) *Locally identifiable* if (28) has a finite number of solutions in $\mathcal{D}$;
3) *Unidentifiable* if (28) has a infinite number of solutions in $\mathcal{D}$.

The SPM is not a linear dynamical model because of its voltage measurement equation (23) incorporating nonlinear Butler–Volmer kinetics (24), (25), and nonlinear OCV functions. Therefore, Definition 1 cannot directly be used to investigate the SPM structural identifiability unless we first linearize the model by assuming a small perturbation around a fixed depth of discharge (DoD) point. Since we assume the nonlinear OCV functions are measured and known *a priori* (for example, using the techniques described in [34] and [35]), linearization is a valid approach to obtain the parameters of the diffusion submodels, which are linear, and to obtain a linearized approximation of the kinetics. The subject of identifiability and parameter estimation of the nonlinear kinetics term in the output equation would be an interesting topic for further research.

A. Diffusion Model Transcendental Transfer Function

Definition 1 requires the model transfer function; we, therefore, first derive this for the spherical particle diffusion model and then combine it in Sections III-B–III-D with the transfer function of the linearized voltage measurement equation to derive the transfer function for the linearized SPM. The transfer function for the spherical diffusion model has previously been derived in the literature for determining the diffusion coefficient of various electrode materials in a laboratory experimental setup [36], [37] and studying the cell frequency response analytically [38], but is included here for completeness. In order to simplify the derivation, the change of variable $\bar{u}_i = \bar{r}\bar{x}_i$ is introduced into the initial-boundary value problem (20)–(22) describing the diffusion in a spherical

particle. Under this change of variable (20) can be equivalently written

$$\frac{\partial \bar{u}_i}{\partial t} = \frac{1}{\tau_i^d} \frac{\partial^2 \bar{u}_i}{\partial \bar{r}^2} \tag{29}$$

and the boundary conditions (21) become

$$\bar{u}_i(\bar{r} = 0) = 0 \quad \text{and} \quad \left. \frac{\partial \bar{u}_i}{\partial \bar{r}} \right|_{\bar{r}=1} - \bar{u}_i(\bar{r} = 1) = \frac{-\tau_i^d}{3Q_i^{\text{th}}} I. \tag{30}$$

Note that the homogeneous Neumann boundary condition at the center of the particle can be reduced to a simpler homogeneous Dirichlet boundary condition so that $\lim_{r_i \to 0} c_i(r_i)$ remains finite. By introducing this change of variable, the initial condition (22) conveniently becomes

$$\bar{u}_i(0, \bar{r}) = 0. \tag{31}$$

Since the initial-boundary value diffusion problem (29)–(31) is linear, an equivalent transfer function can be determined without loss of generality. Taking the Laplace transform of (29) yields

$$\frac{d^2 \bar{U}_i(s, \bar{r})}{d\bar{r}^2} - s\tau_i^d \bar{U}_i(s, \bar{r}) = 0 \tag{32}$$

where s is the frequency-domain Laplace variable. The characteristic equation for this differential equation is

$$\lambda^2 - s\tau_i^d = 0 \quad \Rightarrow \quad \lambda = \pm\sqrt{s\tau_i^d} \tag{33}$$

and its general solution is, therefore,

$$\bar{U}_i(s, \bar{r}) = A_i(s)e^{+\bar{r}\sqrt{s\tau_i^d}} + B_i(s)e^{-\bar{r}\sqrt{s\tau_i^d}} \tag{34}$$

with $A_i(s)$ and $B_i(s)$ two constants (with respect to $\bar{r}$) to be determined using the boundary conditions (30). Substituting (34) into the particle center boundary condition (30) at $\bar{r} = 0$ yields

$$B_i(s) = -A_i(s). \tag{35}$$

And substituting (34) and (35) into the surface boundary conditions (30) at $\bar{r} = 1$ yields

$$A_i(s) = \frac{\tau_i^d}{3Q_i^{\text{th}}} \frac{I(s)/2}{\sinh\left(\sqrt{s\tau_i^d}\right) - \sqrt{s\tau_i^d}\cosh\left(\sqrt{s\tau_i^d}\right)}. \tag{36}$$

Substituting (36)–(35) into (34) yields the general solution

$$\bar{U}_i(s, \bar{r}) = \frac{\tau_i^d}{3Q_i^{\text{th}}} \frac{\sinh\left(\bar{r}\sqrt{s\tau_i^d}\right)}{\sinh\left(\sqrt{s\tau_i^d}\right) - \sqrt{s\tau_i^d}\cosh\left(\sqrt{s\tau_i^d}\right)} I(s). \tag{37}$$

The variable of interest is the surface stoichiometry $\bar{X}_i^s(s)$, rather than $\bar{U}_i(s, \bar{r})$, since this is the variable involved in the voltage measurement equation. By substituting $\bar{u}_i = \bar{r}\bar{x}_i$ into (37), evaluating at $\bar{r} = 1$ and dividing by the input current $I(s)$, the transfer function $H_i^d(s)$ from current to surface stoichiometry for the spherical diffusion model is given as

$$H_i^d(s) = \frac{\bar{X}_i^s(s)}{I(s)} = \frac{\tau_i^d}{3Q_i^{\text{th}}} \frac{\tanh\left(\sqrt{s\tau_i^d}\right)}{\tanh\left(\sqrt{s\tau_i^d}\right) - \sqrt{s\tau_i^d}}. \tag{38}$$

The cathode and anode diffusion transfer functions expressed in terms of the parameter vector $\boldsymbol{\theta}$ are, respectively,

$$H_+^d(s, \boldsymbol{\theta}) = \frac{\theta_2 \tanh(\sqrt{s\theta_1})}{\tanh(\sqrt{s\theta_1}) - \sqrt{s\theta_1}} \tag{39}$$

and

$$H_-^d(s, \boldsymbol{\theta}) = \frac{\theta_5 \tanh(\sqrt{s\theta_4})}{\tanh(\sqrt{s\theta_4}) - \sqrt{s\theta_4}}. \tag{40}$$

B. Linearization of the Voltage Measurement Equation

The voltage measurement equation is a nonlinear function of the anode and cathode surface stoichiometry x_-^s and x_+^s, respectively, and the input current I. Assuming that the input current amplitude I remains small and the battery is operated close to its initial DoD, i.e., the stoichiometry in both electrodes remains close to the initial value x_i^i, the voltage equation can be linearized using a first-order Taylor series approximation about the reference point $\mathbf{x_0} = (x_+^0, x_-^0, I_0 = 0)$ according to

$$\bar{V}^0 \approx \left.\frac{\partial V}{\partial x_+^s}\right|_{\mathbf{x_0}} \bar{x}_+^s + \left.\frac{\partial V}{\partial x_-^s}\right|_{\mathbf{x_0}} \bar{x}_-^s + \left.\frac{\partial V}{\partial I}\right|_{\mathbf{x_0}} I \tag{41}$$

where $\bar{V}^0 = V - V(\mathbf{x_0})$ denotes the deviation of the voltage from the equilibrium voltage at the linearization point

$$V(\mathbf{x_0}) = U_+(x_+^0) - U_-(x_-^0). \tag{42}$$

The partial derivative of the voltage V with respect to the input current I evaluated at the reference point is given as

$$\left.\frac{\partial V}{\partial I}\right|_{\mathbf{x_0}} = \frac{2RT}{\mathcal{F}} \left(\frac{\theta_3}{\sqrt{1 + \frac{(\theta_3 I_0)^2}{(1-x_+^0)x_+^0}} \sqrt{(1-x_+^0)x_+^0}} \right.$$
$$\left. - \frac{\theta_6}{\sqrt{1 + \frac{(\theta_6 I_0)^2}{(1-x_-^0)x_-^0}} \sqrt{(1-x_-^0)x_-^0}} \right) \tag{43}$$

which simplifies to

$$\left.\frac{\partial V}{\partial I}\right|_{\mathbf{x_0}} = \frac{2RT}{\mathcal{F}} \left(\frac{\theta_3}{\sqrt{(1-x_+^0)x_+^0}} - \frac{\theta_6}{\sqrt{(1-x_-^0)x_-^0}} \right) \tag{44}$$

when substituting for $I_0 = 0$. The partial derivative with respect to the surface stoichiometry in the cathode and anode are given, respectively, as

$$\left.\frac{\partial V}{\partial x_+^s}\right|_{\mathbf{x_0}} = +\left.\frac{dU_+}{dx_+^s}\right|_{x_+^s=x_+^0}$$
$$- I_0 \frac{RT}{\mathcal{F}} \frac{\theta_3(1-2x_+^0)}{\sqrt{1 + \frac{(\theta_3 I_0)^2}{(1-x_+^0)x_+^0}}} \left((1-x_+^0)x_+^0\right)^{3/2} \tag{45}$$

and

$$\left.\frac{\partial V}{\partial x_-^s}\right|_{\mathbf{x_0}} = -\left.\frac{dU_-}{dx_-^s}\right|_{x_-^s=x_-^0}$$

$$+ I_0 \frac{RT}{\mathcal{F}} \frac{\theta_6(1-2x_-^0)}{\sqrt{1 + \frac{(\theta_6 I_0)^2}{(1-x_-^0)x_-^0}}} \left((1-x_-^0)x_-^0\right)^{3/2}. \tag{46}$$

Substituting for $I_0 = 0$ yields the simple expressions

$$\left.\frac{\partial V}{\partial x_+^s}\right|_{\mathbf{x_0}} = +\left.\frac{dU_+}{dx_+^s}\right|_{x_+^s=x_+^0} = \alpha_+^0 \tag{47}$$

$$\left.\frac{\partial V}{\partial x_-^s}\right|_{\mathbf{x_0}} = -\left.\frac{dU_-}{dx_-^s}\right|_{x_-^s=x_-^0} = -\alpha_-^0 \tag{48}$$

where α_i^0 denotes the gradients of the OCV functions in each electrode, with respect to stoichiometry, at the linearization point. Substituting the partial derivatives in (41) by their respective expression given by (44), (47), and (48), therefore, yields the linearized voltage measurement equation

$$\bar{V}^0(t) = \alpha_+^0 \bar{x}_+^s(t) - \alpha_-^0 \bar{x}_-^s(t) - R_{\text{ct}}^0(\boldsymbol{\theta})I(t) \tag{49}$$

where $R_{\text{ct}}^0(\boldsymbol{\theta})$ denotes the charge-transfer resistance arising from the intercalation/deintercalation reaction kinetics and defined according to

$$R_{\text{ct}}^0(\boldsymbol{\theta}) = -\frac{2RT}{\mathcal{F}} \left(\frac{\theta_3}{\sqrt{(1-x_+^0)x_+^0}} - \frac{\theta_6}{\sqrt{(1-x_-^0)x_-^0}} \right). \tag{50}$$

C. Transfer Function of the Linearized SPM

Taking the Laplace transform of the linearized voltage equation (49) and dividing by the input current I yields the transfer function $H^0(s, \boldsymbol{\theta}) = \bar{V}^0(s)/I(s)$ of the linearized SPM about the equilibrium point $\mathbf{x_0} = (x_+^0, x_-^0, I_0 = 0)$

$$H^0(s, \boldsymbol{\theta}) = \alpha_+^0 H_+^d(s, \boldsymbol{\theta}) - \alpha_-^0 H_-^d(s, \boldsymbol{\theta}) - R_{\text{ct}}^0(\boldsymbol{\theta}). \tag{51}$$

Substituting for the anode and cathode diffusion transfer function H_+^d and H_-^d with their respective expressions (39) and (40) gives

$$H^0(s, \boldsymbol{\theta}) = \frac{\alpha_+^0 \theta_2 \tanh(\sqrt{s\theta_1})}{\tanh(\sqrt{s\theta_1}) - \sqrt{s\theta_1}}$$
$$- \frac{\alpha_-^0 \theta_5 \tanh(\sqrt{s\theta_4})}{\tanh(\sqrt{s\theta_4}) - \sqrt{s\theta_4}} - R_{\text{ct}}^0(\boldsymbol{\theta}). \tag{52}$$

One can see that only the difference between the parameters θ_3 and θ_6 describing the cathode and anode kinetics appears in the charge-transfer resistance term $R_{\text{ct}}(\boldsymbol{\theta})$ given by (50). As a result, there are an infinite number of pairs (θ_3, θ_6) that will yield the same transfer function and only the lumped parameter R_{ct} can be estimated using the linearized model at a given DoD. We have, therefore, reduced the parameter space to five parameters by combining the cathode and anode kinetics into the charge-transfer resistance term R_{ct}.

This assumes that the OCV slopes α_+^0 and α_-^0 are known parameters, but these are not directly measurable, since in practice, OCV can only be measured with respect to capacity (units: ampere hour or Coulombs), not against stoichiometry (which is nondimensional). By recognizing that the theoretical capacity of an electrode is given by $Q_i^{\text{th}} = c_i^{\text{max}} \mathcal{F} V_i$ with $V_i = \epsilon A \delta_i$ (the volume of active material in the electrode),

TABLE I

PARAMETERS USED FOR GENERATING SYNTHETIC ELECTROCHEMICAL IMPEDANCE DATA FOR AN LCO CELL REPORTED IN [1]

Parameter	Units	Anode	Cathode
Electrode thickness δ_i	μm	73.5	70.0
Particle radius R_i	μm	12.5	8.5
Active material volume fraction ϵ_i	-	0.4382	0.3000
Li diffusivity in active material D_i	$\mathrm{m^2\,s^{-1}}$	5.5×10^{-14}	1.0×10^{-11}
Reaction rate constant k_i	$\mathrm{m^{2.5}\,mol^{-0.5}\,s^{-1}}$	1.764×10^{-11}	6.667×10^{-11}
Max. active material concentration c_i^{max}	$\mathrm{mol\,m^{-3}}$	30 555	51 555
Electrode surface concentration $\mathcal{A}$	$\mathrm{cm^{-2}}$	982	982
Electrolyte concentration c_e	$\mathrm{mol\,m^{-3}}$	1000	

one can easily show that a variation of stoichiometry δx_i is proportional to a variation of charge/discharge capacity δQ according to

$$\delta x_i = \frac{\delta c_i}{c_i^{\max}} = \frac{\delta c_i \mathcal{F} V_i}{Q_i^{\mathrm{th}}} = \frac{\delta Q}{Q_i^{\mathrm{th}}}. \tag{53}$$

Therefore, the derivative of the OCV with respect to x_i can be related to its derivative with respect to charge/discharge capacity Q, denoted β_i^0, according to

$$\beta_i^0 = \frac{\alpha_i^0}{Q_i^{\mathrm{th}}} = \frac{1}{Q_i^{\mathrm{th}}} \left.\frac{dU_i}{dx_i^s}\right|_{x_i^{s,0}} = \left.\frac{dU_i}{dQ}\right|_{x_i^{s,0}}. \tag{54}$$

Substituting α_i^0 for β_i^0 using (54) in (52) and recalling the expressions of Q_i^{th} in terms of θ_j in (27) yields the transfer function

$$H^0(s, \boldsymbol{\theta}) = \beta_+^0 f(s, \theta_1) - \beta_-^0 f(s, \theta_4) - R_{\mathrm{ct}}^0 \tag{55}$$

where the function f defined as

$$f(s, \theta_j) = \frac{1}{3} \frac{\theta_j \tanh(\sqrt{s\theta_j})}{\tanh(\sqrt{s\theta_j}) - \sqrt{s\theta_j}} \tag{56}$$

is only parametrized by the electrode diffusion time constant θ_1 or θ_4 in the cathode or anode, respectively. The coefficients β_+^0 and β_-^0 are the measurable and assumed known OCV gradients with respect to capacity in the cathode and anode, respectively. This requires access to half-cell or reference electrode cell data, which may be obtained from commercially available cells as we have recently demonstrated [34], [35]. In the absence of individual electrode OCV data, it is not possible to parametrize the SPM directly, although it may be reasonable to use a two electrode OCV measurement combined with available OCV data from the literature for the graphite negative electrode to infer the positive electrode OCV function.

We have thus reduced the parameter estimation problem of the linearized SPM to three independent parameters: the cathode diffusion time constant $\theta_1 = \tau_+^d$, the anode diffusion time constant $\theta_4 = \tau_-^d$, and the charge-transfer resistance R_{ct}. We will subsequently define the vector $\tilde{\boldsymbol{\theta}} \in \mathbb{R}^3$ of identifiable parameters as

$$\tilde{\boldsymbol{\theta}} = \begin{bmatrix} \tau_+^d & \tau_-^d & R_{\mathrm{ct}}^0 \end{bmatrix}^T. \tag{57}$$

The transfer function of the linearized SPM expressed in terms of the three parameters defined in $\tilde{\boldsymbol{\theta}}$ is given as

$$H^0(s, \tilde{\boldsymbol{\theta}}) = \beta_+^0 f(s, \tau_+^d) - \beta_-^0 f(s, \tau_-^d) - R_{\mathrm{ct}}^0. \tag{58}$$
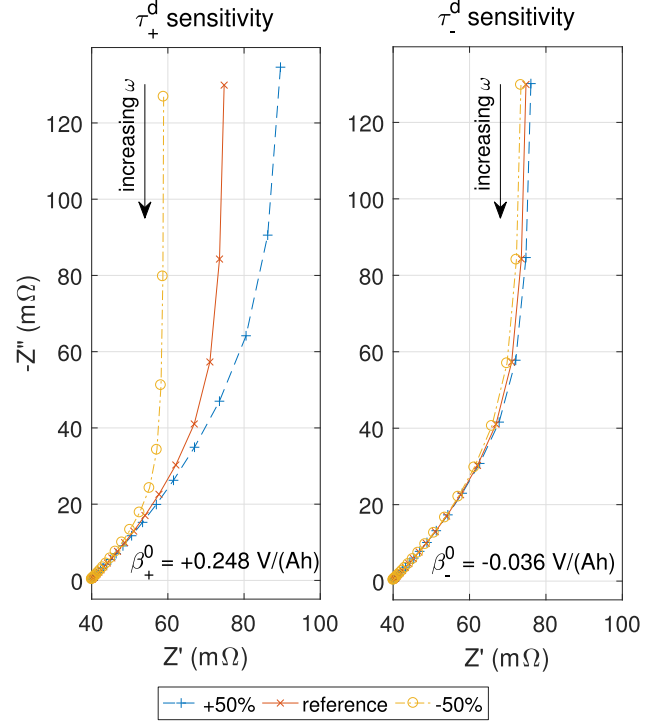

Fig. 1. Comparison of the Nyquist frequency response predicted by the transfer function (58) using the reference parameters given in Table I with (left) the cathode diffusion time constant τ_+^d and (right) the anode diffusion time constant τ_-^d varied by ±50% from their nominal values. The OCV slope values β_i^0 corresponding to the chosen linearization point (DoD = 25%) are indicated on the graph for each electrode.

Fig. 1 shows a Nyquist plot of the SPM frequency response predicted by (58) at 25% DoD for the lithium cobalt oxide (LCO) cell parameters given in Table I. At low frequencies, the response features a 45° slope that is representative of semiinfinite linear diffusion. This 45° slope is commonly referred to as the "diffusion tail" in the battery EIS community and is usually modeled using a so-called Warburg constant-phase element [27], [39]. The cell frequency response tends toward a capacitive behavior with decreasing frequency as exhibited by the vertical asymptote on the Nyquist plot. This capacitive behavior arises from the variation of the average particle concentration at low frequencies, as opposed to the surface concentration variation only, due to the finite-length nature of the diffusion problem. Although the low frequencies giving rise to this capacitive behavior are usually avoided

in the lithium-ion battery EIS literature, we argue that the departure from the semiinfinite diffusion 45° tail actually provides a more informative data set for the parameter estimation of the SPM. Fig. 1 also shows the effect of varying the diffusion time constants τ_+^d and τ_-^d in the cathode and anode, respectively, by $\pm 50\%$ from their nominal values. Generally, a larger diffusion time constant (slower diffusion) yields higher cell impedance as expected. Moreover a smaller diffusion time constant (faster diffusion) results in the capacitive behavior occurring at higher frequencies; this is because faster diffusion results in easier variations of the average particle concentration. Finally, the frequency response is much more sensitive to the cathode diffusion than the anode diffusion at this DoD because of the flat anode OCV curve here, as shown by the low value of the anode OCV slope β_-^0 compared to β_+^0. This behavior will be explained in more detail in the subsequent sections.

D. Structural Identifiability Analysis

Definition 1 can now be applied to the SPM transfer function (58). To check the structural identifiability of the linearized model, we need to show that

$$\begin{aligned}
\beta_+^0 f\left(s, \tau_+^d\right) &- \beta_-^0 f\left(s, \tau_-^d\right) - R_{ct}^0 \\
&= \beta_+^0 f\left(s, \tau_+^{d*}\right) - \beta_-^0 f\left(s, \tau_-^{d*}\right) - R_{ct}^{0*}
\end{aligned} \quad (59)$$

for almost all s, implies the parameters equality

$$\begin{bmatrix} \tau_+^d & \tau_-^d & R_{ct}^0 \end{bmatrix}^T = \begin{bmatrix} \tau_+^{d*} & \tau_-^{d*} & R_{ct}^{0*} \end{bmatrix}^T. \quad (60)$$

Because the charge-transfer resistance is the only additive parameter independent of s on both sides of the equation, we clearly have $R_{ct}^0 = R_{ct}^{0*}$, and the structural identifiability equation reduces to

$$\beta_+^0 f\left(s, \tau_+^d\right) - \beta_-^0 f\left(s, \tau_-^d\right) = \beta_+^0 f\left(s, \tau_+^{d*}\right) - \beta_-^0 f\left(s, \tau_-^{d*}\right) \quad (61)$$

for almost all s. Since f is a nontrivial function of s, this equality holds in the general case for most values of s, if and only if $\tau_+^d = \tau_+^{d*}$ and $\tau_-^d = \tau_-^{d*}$, and so the linearized SPM is structurally identifiable. There are, however, a few cases where other solutions exist in the following.

1) If $\beta_+^0 = 0$ (respectively, $\beta_-^0 = 0$), then any pair (τ_+^d, τ_+^{d*}) [respectively, (τ_-^d, τ_-^{d*})] satisfy the identifiability equation and the linearized SPM becomes unidentifiable. This makes sense because a "flat" OCV function hides any diffusion dynamics effect of that electrode as shown in Fig. 1 for the anode diffusion when $\mid \beta_-^0 \mid \ll \mid \beta_+^0 \mid$.

2) If the magnitudes of the OCV function in each electrode are equal $\beta_+^0 = -\beta_-^0 = \beta^0$, then interchanging the diffusion time constants $\tau_+^d = \tau_-^{d*}$ and $\tau_-^d = \tau_+^{d*}$ satisfies the structural identifiability equation, and the linearized SPM is structurally identifiable provided the diffusion time constants are ordered.

In conclusion, the linearized SPM is structurally identifiable in the general case. In practice, the fact that a "flat" OCV function results in unidentifiable parameters is not problematic since identification may be performed using data at several DoDs,

ensuring the OCV functions have a significant slope in each electrode.

IV. FREQUENCY-DOMAIN PARAMETER ESTIMATION

This section discusses the implementation of the estimation algorithm for the transfer function of the linearized SPM from frequency-domain EIS experimental data. The experimental methodology is discussed in Section V. We define the vector $\boldsymbol{\theta}_{id}$ of parameters identified by the estimation algorithm in the general sense, where $\boldsymbol{\theta}_{id}$ could be equal to the full vector of parameters $\boldsymbol{\theta}$ given by (26) or a subset of parameters such as $\tilde{\boldsymbol{\theta}}$ given by (57). The estimation is performed by finding the best fit in the least-squares sense, i.e., by minimizing the sum of squared errors between both the real and imaginary parts of the experimental and predicted impedances over a number of frequencies [32]. First, the loss function for the estimation at a single DoD is presented and extended to simultaneous estimation at several DoDs. Then, we show how all combined purely resistive parameters, including charge-transfer resistance R_{ct}, can be estimated separately by simple linear regression at a given DoD.

A. Single DoD Parameter Estimation

The measured impedance of a cell at a given frequency ω_i is denoted by the complex number $Z_j(\omega_i) = Z_j'(\omega_i) + i Z_j''(\omega_i)$, where Z' and Z'' denote the real and imaginary parts, respectively, and the subscript j denotes the DoD. Similarly, the impedance predicted by the SPM will be denoted $H_j(\omega_i, \boldsymbol{\theta}_{id})$ in Sections IV-B and IV-C.

The optimal parameter estimate in the least-squares (the maximum likelihood) sense is given by the estimator $\hat{\boldsymbol{\theta}}_{id}$ that minimizes the loss function $L_j(\boldsymbol{\theta}_{id})$ according to

$$\hat{\boldsymbol{\theta}}_{id} = \arg \min_{\boldsymbol{\theta}_{id}} L_j(\boldsymbol{\theta}_{id}) \quad (62)$$

where the loss function is the sum over N_ω chosen frequencies of the squared magnitude of the error between predicted and measured complex impedance according to

$$L_j(\boldsymbol{\theta}_{id}) = \sum_{i=1}^{N_\omega} |Z_j(\omega_i) - H_j(\omega_i, \boldsymbol{\theta}_{id})|^2. \quad (63)$$

This is also equal to the sum of the squared real and imaginary part errors according to

$$\begin{aligned}
L_j(\boldsymbol{\theta}_{id}) = &\sum_{i=1}^{N_\omega} \left(Z_j'(\omega_i) - H_j'(\omega_i, \boldsymbol{\theta}_{id}) \right)^2 \\
&+ \sum_{i=1}^{N_\omega} \left(Z_j''(\omega_i) - H_j''(\omega_i, \boldsymbol{\theta}_{id}) \right)^2. \quad (64)
\end{aligned}$$

B. Combined DoDs Parameter Estimation

As mentioned in Section III-D and shown in Section V, the estimation of the parameter $\tilde{\boldsymbol{\theta}}$ based on the impedance data at a single DoD may be unidentifiable in practice due to the flatness of one of the electrode OCV functions. Therefore, the parameter estimation must be performed against

impedance measured at several DoDs. As before, the optimal parameter estimate is given by the argument $\hat{\boldsymbol{\theta}}_{\mathrm{id}}$ minimizing the loss function according to

$$\hat{\boldsymbol{\theta}}_{\mathrm{id}} = \arg\min_{\boldsymbol{\theta}_{\mathrm{id}}} L(\boldsymbol{\theta}_{\mathrm{id}}) \tag{65}$$

where the loss function $L(\boldsymbol{\theta}_{\mathrm{id}})$ in this case is simply defined as the sum of the loss functions L_j defined in (64) over N_{DoD} levels of DoD, where j denotes the DoD, according to

$$L(\boldsymbol{\theta}_{\mathrm{id}}) = \sum_{j=1}^{N_{\mathrm{DoD}}} \sum_{i=1}^{N_\omega} |Z_j(\omega_i) - H_j(\omega_i, \boldsymbol{\theta}_{\mathrm{id}})|^2. \tag{66}$$

C. Estimation of Purely Resistive Terms Including Charge-Transfer Resistance

Although the simultaneous parameter estimation at several DoDs could in theory improve the identifiability of the estimation problem (assuming the diffusion parameters are not a function of DoD), it also adds N_{DoD} charge-transfer resistances R_{ct}^0 to identify because of the dependence of R_{ct}^0 on stoichiometry (or equivalently DoD) in (50). The charge-transfer resistance R_{ct}^0 is an additive purely resistive term in the transfer function describing the cell impedance. Therefore, its only effect is to shift the impedance response along the real axis on the Nyquist plot. In order to reduce the parameter space to be explored, a purely resistive term denoted R_0, combining the higher frequency charge-transfer resistance R_{ct}^0, the ohmic contact resistance of the cell and any resistive effect due to passivation layers, can be estimated separately by simple linear regression and subtracted from the experimental frequency-response data. Recalling from Section III-C that the semiinfinite diffusion-driven impedance at lower frequencies features a characteristic $45°$ slope, the charge-transfer resistance can be estimated by fitting a $45°$ straight line to the experimental response at lower frequencies, and extrapolating to find the intercept of this with the real axis on the Nyquist diagram. Although the SPM could be extended to account for double-layer capacitance effects, this is beyond the scope of this paper. Therefore, the semicircle at higher frequencies on the experimental EIS Nyquist plot, which arises from the parallel combination of charge-transfer resistance and double-layer capacitance, is ignored. Any high-frequency effects are considered as purely resistive and accounted for in the term R_0 estimated by the linear regression described as follows. We assume that any experimental high-frequency data points, where charge-transfer processes are dominant (charge-transfer semicircle), have been removed; only data points at frequencies where diffusion processes are dominant remain. The linear regression for estimating the purely resistive term is discussed in Section V-B.2.

Denoting $x_i = Z'(\omega_i)$ and $y_i = -Z''(\omega_i)$, the real part and negative imaginary part, respectively, of the experimental impedance at frequency ω_i, the linear regression problem is

$$y_i = \beta_1 x_i + \beta_0. \tag{67}$$

The slope is set to $45°$ to represent the diffusion behavior as discussed earlier. Therefore, $\beta_1 = 1$ is known and the regression problem consists of estimating the real intercept β_0 $(= -R_0)$ only. Defining the variable $\bar{y}_i = y_i - \beta_1 x_i$, the regression problem can be written

$$\bar{y}_i = \beta_0. \tag{68}$$

This, therefore, constitutes an overdetermined system of N_ω equations with the only unknown β_0, which can be written

$$\bar{\mathbf{Y}} = \beta_0 \mathbf{1} \tag{69}$$

where $\bar{\mathbf{Y}} = [\bar{y}_1, \ldots, \bar{y}_{N_\omega}]^T \in \mathbb{R}^{N_\omega}$ is the vector containing the values of $\bar{y}_i$ at the N_ω frequencies, and $\mathbf{1} \in \mathbb{R}^{N_\omega}$ is a vector of all ones of length N_ω. The value of β_0 can easily be determined in the least-squares sense by computing

$$\beta_0 = \mathbf{1}^\dagger \bar{\mathbf{Y}} = \frac{\mathbf{1}^T}{N_\omega} \bar{\mathbf{Y}} \tag{70}$$

where the superscript $\mathbf{1}^\dagger$ denotes the pseudoinverse of the vector $\mathbf{1}$ that is simply equal to a row vector with all components equal to $1/N_\omega$. This linear regression must be performed using only the experimental data points in the frequency range where low-frequency pseudocapacitive effects arising from OCV variations are negligible. Therefore, very low frequency impedance data points must be discarded in the experimental data set to perform a meaningful regression. In practice, this was achieved by performing the regression first on all data points, and then on an iteratively reduced data set where the lowest frequency impedance data point was removed until the goodness of fit was satisfactory. The coefficient of determination R^2 was used as an indicator to assess the goodness of fit and a threshold value of 0.98 was chosen to stop the iterations.

V. RESULTS AND DISCUSSION

A. Parameter Estimation Using Synthetic Data

The parameter estimation algorithm was first tested against synthetic data generated using the linearized SPM with a known set of parameters for an LCO cell from the literature [1], which are summarized in Table I.

Fig. 2 shows contour plots of the natural logarithm of the loss function $L_j(\tilde{\boldsymbol{\theta}})$, (64), at several DoDs for the synthetic data. It is assumed that the charge-transfer resistance R_{ct} is known for each DoD since, as explained earlier, it can be identified separately by straightforward linear regression. Therefore, the two parameters to be identified are the cathode and anode diffusion time constants τ_+^d and τ_-^d, respectively. The coordinates of the minimum values of the natural logarithm of (64) on these contour plots represent the optimal parameter estimates in the least-squares sense as defined in (62). The two cases for which the linearized SPM is structurally unidentifiable, as discussed in Section III-D, can be witnessed by examining Fig. 2. First, when the absolute value of the OCV functions is approximately equal in the cathode and anode, $\beta_+^0 \approx -\beta_-^0$, such as 75% DoD, the loss function clearly shows two minima: one minimum corresponds to the actual parameters, while the other minimum happens when the anode and cathode diffusion time constants are interchanged. Moreover, even if the absolute values of the
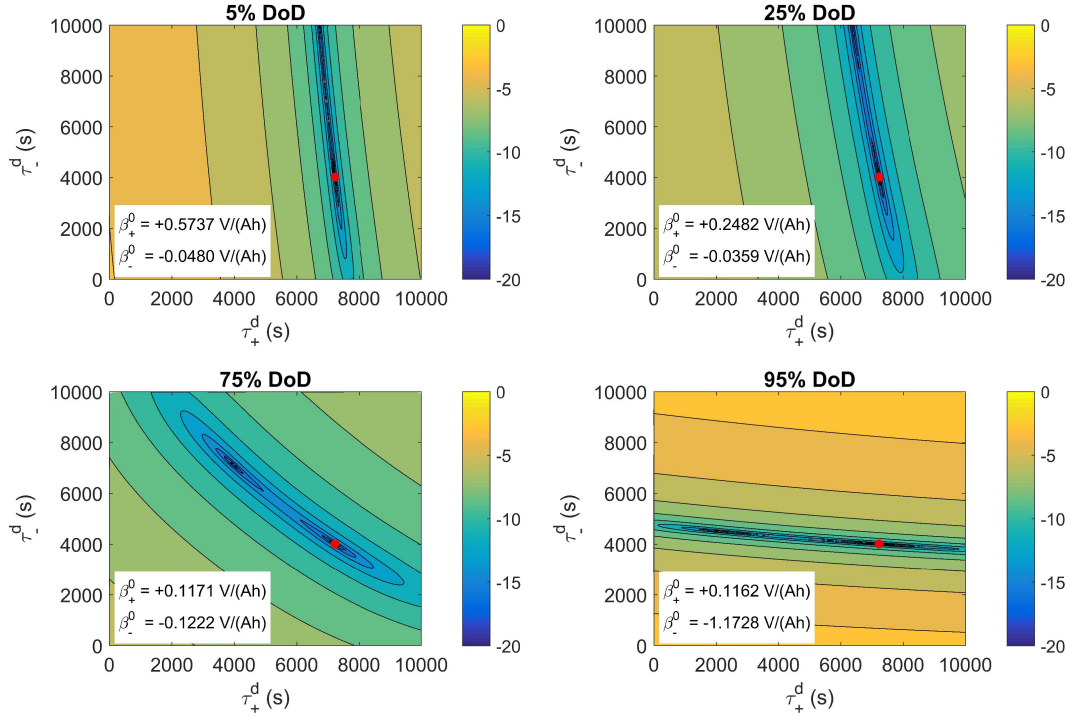
Fig. 2. Contour plots of $\ln L_j(\tilde{\boldsymbol{\theta}})$ against (τ_+^d, τ_-^d) at several DoDs assuming the charge-transfer resistance R_{ct} is known. Synthetic EIS data were generated using the linearized SPM with reference parameters found in the literature [1] for an LCO cell (shown as a red dot on the contour plot).

electrode OCV slopes β_-^0 and β_+^0 are distinct (e.g., 5%, 25%, and 95% in Fig. 2), the loss function still features two local minima, although barely visible due to the narrow loss function along one axis. Therefore, an ambiguity persists and the anode and cathode dynamics cannot be distinguished. A possible explanation for this ambiguity is that the measured voltage is the difference between the anode and cathode OCV and not the absolute voltage of the electrode with respect to a reference electrode. Second, in the case where one OCV slope is an order of magnitude lower in one electrode compared to the other, the diffusion time constant of this electrode becomes unidentifiable, e.g., 5%, 25%, and 95% DoD in Fig. 2. For instance at 95% DoD, the absolute value of the cathode OCV slope β_+^0 is small compared to the anode slope, and the minimum of the loss function is elongated along the τ_+^d axis, i.e., provided the value of τ_-^d is correct, almost any value for τ_+^d will result in a minimum value of the loss function.

These results suggest that both the anode and cathode diffusion time constants cannot be identified from frequency data at a single DoD. In the best case, where the OCV slopes are equal for the chosen DoD, the values τ_+^d and τ_-^d can be determined but cannot be assigned to a specific electrode. Fig. 3 shows the natural logarithm of the loss function $L(\tilde{\boldsymbol{\theta}})$ combining the EIS data at 5%, 25%, 75%, and 95% DoD as defined in (66). This loss function shows a single global minimum corresponding to the actual set of parameters used to generate the synthetic data. The two time constants of the linearized SPM can, therefore, only be estimated unambiguously by considering EIS data at several DoDs. More specifically, complementary DoD values, where each electrode in turn presents a large OCV slope while the other is negligible, should be combined to ensure
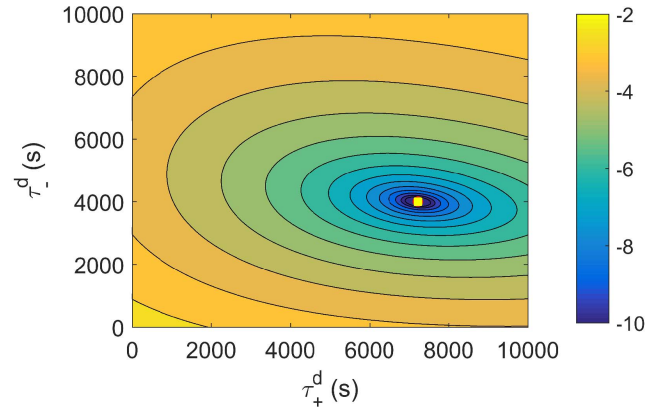

Fig. 3. Contour plots of $\ln L(\tilde{\boldsymbol{\theta}})$ against (τ_+^d, τ_-^d) assuming the charge-transfer resistance R_{ct} is known, based on synthetic EIS data with the reference parameters from [1] for an LCO cell (shown as a yellow square on the contour plot). The loss function is the sum of the cost function L_j for four levels of DoD 5%, 25%, 75%, and 95%.

better identifiability. For instance, it is clear from Fig. 2 that combining EIS data at 5% and 95% DoD will result in a single minimum at the intersection of the lines of minimum loss function values for individual DoDs.

B. Parameter Estimation Using Experimental Data

This section discusses the results of the parameter estimation using EIS experimental data measured from a commercial Kokam nickel manganese cobalt (NMC) cell (note that the model parameter values given in Table I are for an LCO cell and are, therefore, not directly relatable to this NMC

cell). First, the experimental procedure used to measure the cell impedance and the OCV for both electrodes is discussed. The estimation of the charge-transfer resistance using linear regression is then briefly considered. Finally, the practical identifiability of the model diffusion time constants from the experimental impedance data is examined.

1) Experimental Setup: EIS [27] is a widely used technique to measure the frequency response of electrochemical systems, including lithium-ion batteries. During a galvanostatic EIS (GEIS) experiment, the battery is excited with a small sinusoidal current and the associated voltage response is recorded. This is repeated at a number of frequencies. Potentiostatic EIS is a similar technique, where the voltage is used as the input sinusoidal signal and the recorded output is the current. The impedance of the cell at each frequency is calculated from the gain and phase shift between the input and output signals. EIS experimental data were obtained for a Kokam SLPB533459H4 740-mAh NMC cell at several DoDs using a BioLogic SP-150 potentiostat. The cell was kept at a constant 20 °C temperature in a Vötsch VT4002 thermal chamber in order to minimize the possible detrimental effects of temperature variations on the results of the parameter identification approach. The cell impedance was measured using single-sine GEIS, averaged over two periods, with a peak-to-peak ac current amplitude of 100- and 0-mA dc current. The impedance was measured at logarithmically spaced frequencies with six frequencies per decade ranging from 5 kHz to 200 μHz. A resting time of 3 h was applied before any EIS measurement to ensure that the cell was close to equilibrium. The EIS measurement using this experimental setup took approximately 9 h for each DoD because of the low frequencies required. Clearly, this is quite time consuming and ultimately one should aim at using the minimum number of low-frequency data and/or DoD linearization points to accelerate the model parametrization.

Fig. 4 shows the measured EIS data as a Nyquist plot for several DoDs ranging from 10% to 90%. These impedance results are typical of lithium-ion batteries, which have smaller impedance at high frequencies (bottom left), arising from ohmic resistance and fast charge-transfer processes, and larger impedance at lower frequencies (top right), arising from slower diffusion processes and SoC variations. At high frequencies, the response features a depressed semicircle, which is characteristic of charge-transfer processes. As discussed in Section IV-C, this part of the plot is discarded because charge-transfer processes are approximated by the resistor R_{ct}^0 only in (58). As expected, in the medium range of frequencies where semiinfinite diffusion is predominant, the frequency response shows the familiar 45° diffusion slope. At very low frequencies, the response tends toward a capacitive vertical line due to the variations of the average particle stoichiometry.

Fig. 5(d) shows the OCV of the Kokam SLPB533459H4 cell as a function of discharge capacity Q and DoD measured experimentally. In order to measure the anode and cathode potential separately, a minimally invasive reference electrode consisting of a lithium-coated copper wire was inserted into the commercial pouch cell using the technique presented in [35]. The OCV of both electrodes were then measured using
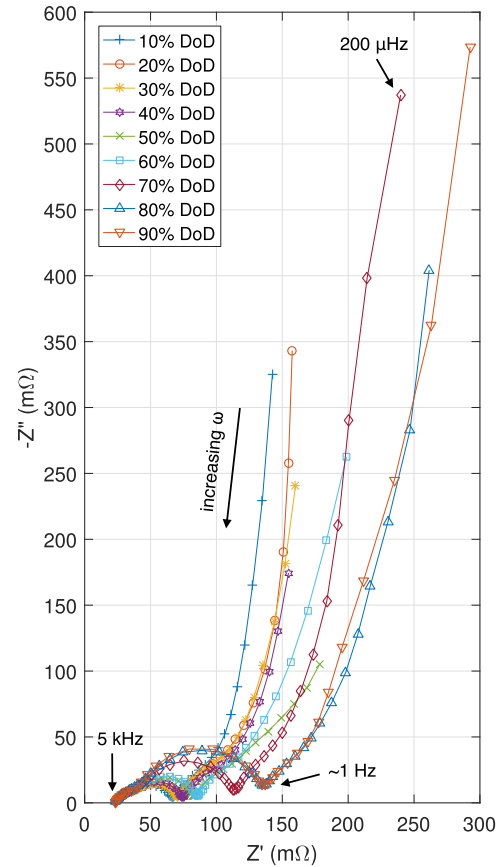

Fig. 4. Nyquist plot of the electrochemical impedance of a Kokam SLPB533459H4 740-mAh NMC cell measured at 20 °C and several DoDs in the frequency range 5 kHz to 200 μHz.

the galvanostatic intermittent titration technique (GITT) [34] by discharging the cell in 14.8-mAh increments at C/10 and measuring the cell OCV after a 1-h voltage relaxation time to obtain 50 measurements points.

2) Estimation of High-Frequency Purely Resistive Terms: The purely resistive term R_0 accounting for high-frequency effects, including charge-transfer, passivation layer, and contact resistance, which shifts the diffusion-driven impedance to the right on the experimental EIS Nyquist plot, is estimated using the linear regression method discussed in Section IV-C. Fig. 6 shows the results of the linear regression for the EIS data collected at 10% DoD. As discussed earlier, high-frequency data points corresponding to charge-transfer resistance and double-layer capacitance are discarded and only data points at frequencies where diffusion effects are predominantly considered. The initial linear regression is performed on all low-frequency data points but yields very poor fitting ($R^2 = 0.525$) due to the pseudocapacitive behavior at very low frequencies arising from the DoD variations. By iteratively removing the lower frequency data points, a good linear fit of the 45° tail can be achieved ($R^2 = 0.995$). The purely resistive term R_0 is then approximated by finding the intercept of the linear regession curve with the real axis. The estimated values of R_0 as a function of the DoD are reported in Fig. 7. Note that the cell ohmic resistance included in R_0 is approximately equal
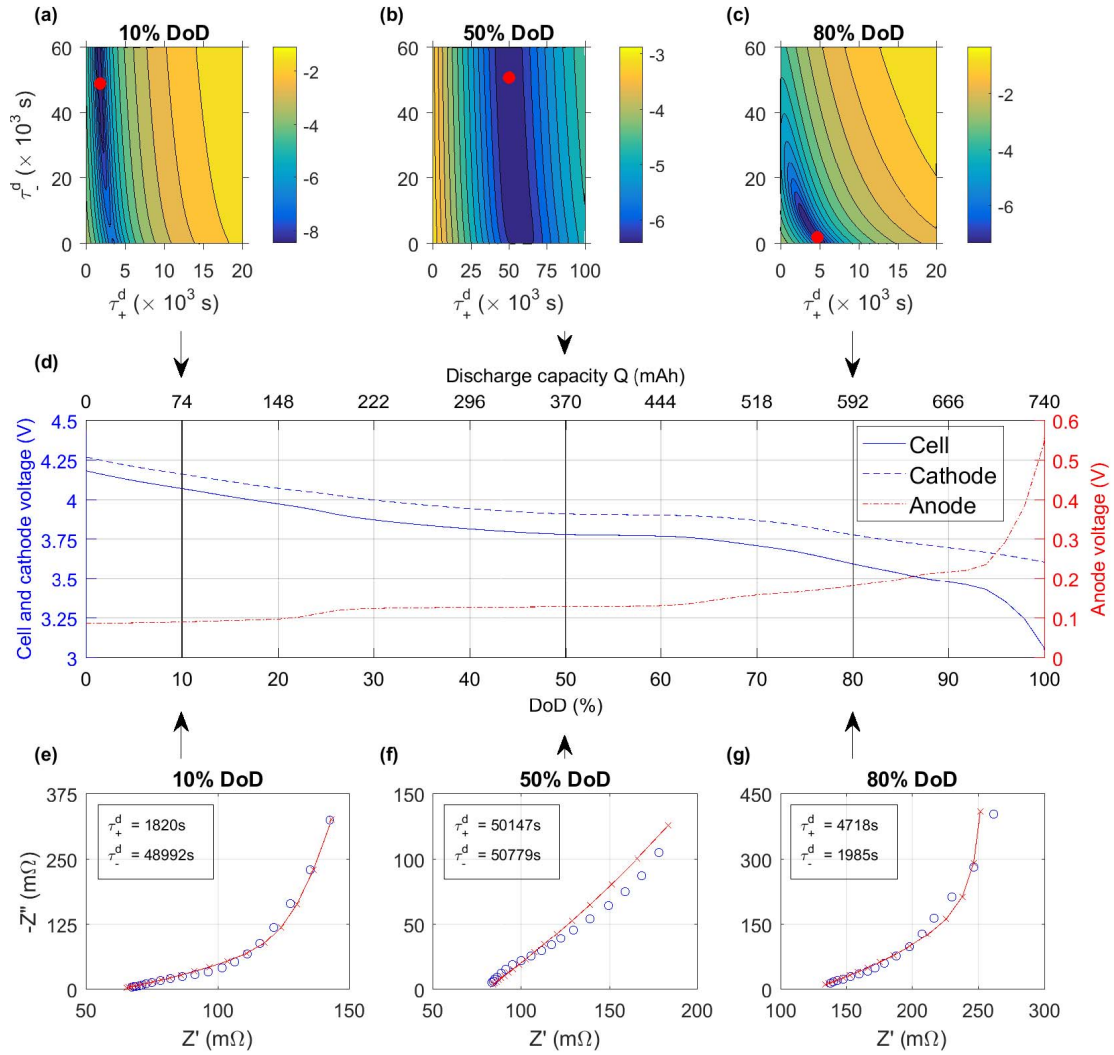
Fig. 5.   Natural logarithm of the individual DoD loss function $L_j(\tilde{\boldsymbol{\theta}})$ based on experimental EIS data at (a) 10%, (b) 50%, and (c) 80% DoD. (d) Cathode, anode, and cell OCV of the Kokam cell as a function of DoD measured by the GITT technique using a minimally invasive reference electrode. Cell impedance experimentally measured (circles) and predicted (solid lines and crosses) by the linearized SPM transfer function model fit by minimizing the individual DoD loss function $L_j(\tilde{\boldsymbol{\theta}})$ at (e) 10%, (f) 50%, and (g) 80% DoD.

TABLE II

RMS AND MAXIMUM ERROR BETWEEN THE MEASURED AND PREDICTED IMPEDANCE AT 10%, 50%, AND 80% DoD

DoD	Single DoD estimation		Combined DoDs estimation	
	RMS Error	Max Error	RMS Error	Max Error
10 %	3.28 mΩ	5.60 mΩ	6.66 mΩ	16.73 mΩ
50 %	9.56 mΩ	21.36 mΩ	47.88 mΩ	95.16 mΩ
80 %	6.48 mΩ	11.32 mΩ	6.84 mΩ	12.82 mΩ

to 25 mΩ according to the intercept of the experimentally measured impedance with the real axis of the Nyquist plot at high frequencies, Fig. 4. As shown, the resistive term R_0 including charge-transfer and contact resistance increases with the DoD, which is consistent with previously reported Kokam NMC cell EIS data in the literature [40].

3) Parameter Estimation Performance: Fig. 5 presents practical identifiability and parameter estimation results based on experimental impedance data at individual DoDs. Three

characteristic values of DoD were chosen, 10%, 50%, and 80%, in order to demonstrate the identifiability issues discussed in Section III-D. At 10% DoD, only the cathode OCV shows a significant slope, at 50% DoD both the cathode and anode OCV are flat, and at 80% DoD both electrodes feature a significant OCV slope. The experimental and fit impedance responses are shown in Fig. 5(e)–(g) for the chosen values of DoD. The corresponding root-mean square (rms) and maximum (Max) errors between the predicted and measured impedance response for this single DoD parameter estimation algorithm are presented in Table II. A satisfactory fit is obtained in all cases with a rms error of 3.28, 9.56, and 6.48 mΩ for 10%, 50%, and 80% DoD, respectively.

However, the uncertainties on the parameter estimates are large as exhibited by the contour plots of the loss function in Fig. 5(a)–(c). At 10% DoD, the loss function is very sensitive to the cathode diffusion dynamics while anode dynamics have very little impact because of the very small slope of the anode OCV. Therefore, the estimated anode diffusion time
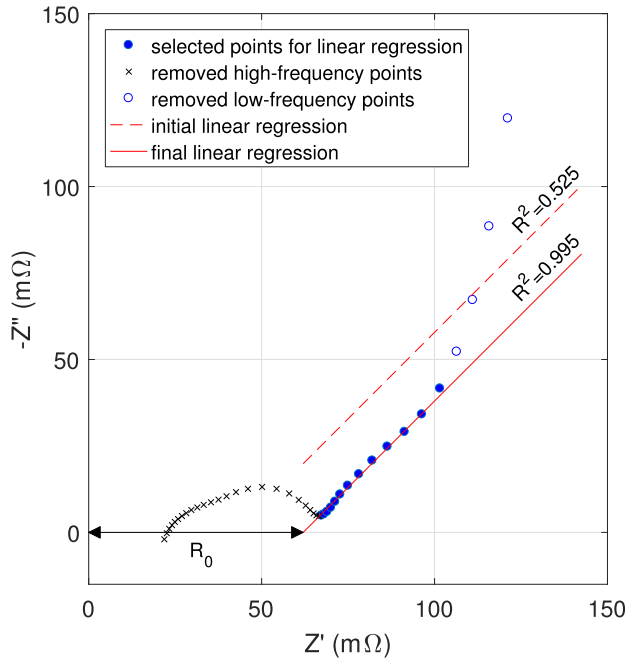
Fig. 6. Linear regression of the purely resistive term R_0 from experimental EIS data at 10% DoD. The high-frequency data points (crosses) are discarded. The first linear regression (dashed line) is performed on all data points (circles). Low-frequency data points (empty circles), corresponding to the pseudocapacitive effect arising from DoD variations, are iteratively removed until the final remaining set of data points (filled circles) enables a linear regression with a coefficient of determination R^2 greater than 0.98 (the three lowest frequency data points are not shown on this graph for readability).
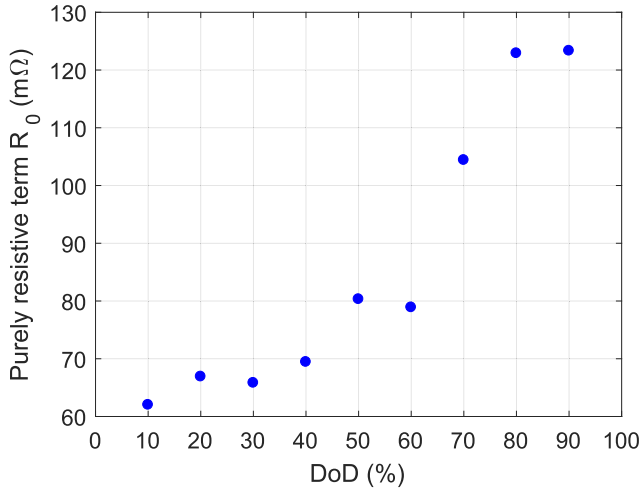

Fig. 7. Purely resistive term R_0, accounting for charge-transfer, passivation layer, and contact resistance at high frequencies, against DoD estimated from experimental data by linear regression.

constant τ_-^d is highly uncertain and cannot be estimated from this data set alone. In contrast, at 80% DoD the loss function is sensitive to both the anode and cathode dynamics because of the similar magnitude of the OCV slope in both electrodes. However, the minimum of the loss function is still relatively elongated along the anode parameter axis, which suggests that the uncertainty on the anode parameter remains larger than the cathode one. This confirms that impedance data at several
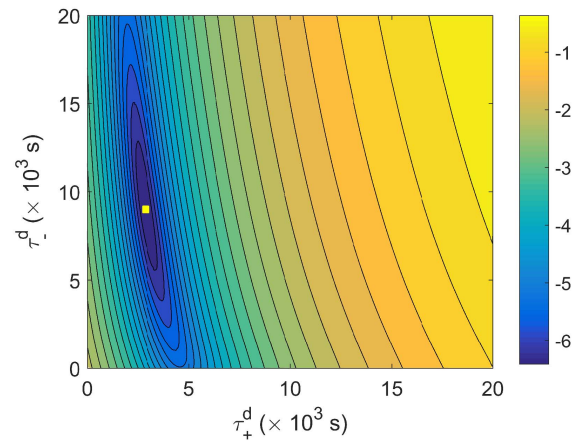

Fig. 8. Contour plot of the loss function $\ln L(\tilde{\boldsymbol{\theta}})$, (66), based on experimental impedance data at 10% and 80% DoD. Yellow square: parameter estimated by the PE algorithm at $\tau_+^d = 2880$ s and $\tau_-^d = 9033$ s.

DoDs must be combined to yield less uncertain parameter estimates.

At 50% DoD, where the OCV is flat for both electrodes, the loss function is completely insensitive to the anode dynamics and somewhat more sensitive to the cathode dynamics. However, the contour plot of the loss function is actually shallow along the cathode parameter as well, implying that the uncertainty on both the parameters is very large. Furthermore, the minimum of the loss function happens for a cathode diffusion time constant centered around 60 000 s as shown in Fig. 5(b). This is approximately an order of magnitude higher than the value of τ_+^d estimated using the other data sets at 10% and 80% DoD. Throughout this paper, the implicit assumption was made that both diffusion time constants do not vary with DoD. However, Fig. 5(b) suggests that lithium diffusivity in the electrode active material could drastically change with DoD. Experimental measurements of lithium diffusivities in the active material of a Kokam NMC cell are reported in [41] and confirm this. More especially, both the anode and cathode diffusivities are an order of magnitude lower around 50% DoD compared to high DoDs [41]. Another source of uncertainty that has been ignored in the model is the error related to the OCV measurement and the calculation of the OCV slopes β_+^0 and β_-^0. At 50% DoD, the OCV slopes in both electrodes are very small, and therefore, the relative error on measurement is large, especially considering that numerical differentiation is highly sensitive to noise. Finally, because the OCV slopes are flat, both the anode and cathode diffusion dynamics have very limited impact on the cell terminal voltage at 50% DoD. Therefore, the EIS data at 50% DoD will be discarded from the parameter estimation using combined DoDs discussed subsequently.

Fig. 8 shows the contour plot of the cost function $L(\tilde{\boldsymbol{\theta}})$ combining the experimental impedance data measured at 10% and 80% DoDs. Similar to the results with synthetic data, Fig. 3, the loss function presents a single minimum, elongated along the anode parameter axis suggesting a larger uncertainty on the anode parameter compared to the cathode one. Although this

suggests a "well-behaved" estimation problem with a single parameter estimate, these results must be considered with caution. Indeed, the two combined data sets at 10% and 80% DoDs used to perform the parameter estimation were chosen somewhat arbitrarily. Although these parameter estimates yield a good impedance fit for these DoDs, it results in very approximate fit impedance at other DoDs, e.g., 50% DoD. As given in Table II, the impedance prediction error is much higher at 50% DoD with 47.88-mΩ rms error compared to 6.66 and 6.84 mΩ at 10% and 80% DoDs, respectively. First, as mentioned earlier, the OCV slopes β_i^0 in both electrodes are assumed fixed and perfectly known for each DoD. The sensitivity of the predicted impedance response to the OCV slopes is not negligible. The computation of the OCV slope is highly sensitive to measurement noise because the measured voltage variations are relatively small between each DoD, on the order of a few millivolts. In addition, the measured OCV might not reflect closely enough the actual cell OCV. The OCV measurements were performed on a different cell (of the same type and size) that was modified by inserting a reference electrode. Although this technique is minimally invasive, it nonetheless may slightly modify the cell behavior. Finally, electrode OCV is affected by temperature variation and hysteresis effects [34], which introduce further uncertainties. Second, our parameter estimation algorithm combining experimental data at several DoDs assumes that the diffusion time constants in both electrodes remain constant with DoD. Although solid-phase diffusivities are usually assumed constant with respect to active material lithiation in the lithium-ion battery electrochemical modeling community (see [1], [14], [15], [42], [43]), this assumption may introduce additional inaccuracies on the parameter estimate, especially for NMC cells [41]. All of these challenges provide fruitful avenues for further exploration.

C. Model Validation in the Time Domain

To demonstrate the performance of the linearized SPM using our frequency-domain parameter estimation approach, we also include here a brief comparison between the modeled and measured voltage response in the time domain. The measurements were made on the same Kokam cell type as described earlier, using the same equipment that was used for EIS measurements. The current demand was specified based on a dynamic loading profile at 1 Hz derived from an electric vehicle drive cycle (see [44]). The maximum current was 4.4 A, which corresponds to a fairly high *C*-rate (almost 6*C*). The same current input signal used in the experimental measurements was provided to the linearized SPM, and the terminal voltage was calculated by solving the model in the time domain. This requires solution of (29)-(31), (49), (54), which requires knowledge of Q_i^{th}, the theoretical capacity of each electrode, which relates variations in stoichiometry x to variations in measured discharge capacity. Unfortunately, Q_i^{th} is unknown, but by introducing two changes of variable, $\hat{u}_i = Q_i^{th}\bar{u}_i$ and $\hat{x}_i^s = Q_i^{th}\bar{x}_i^s$, this term can be eliminated from the linearized SPM, similar to Section III-C. This approach assumes the model is linearized; to run the SPM with nonlinear
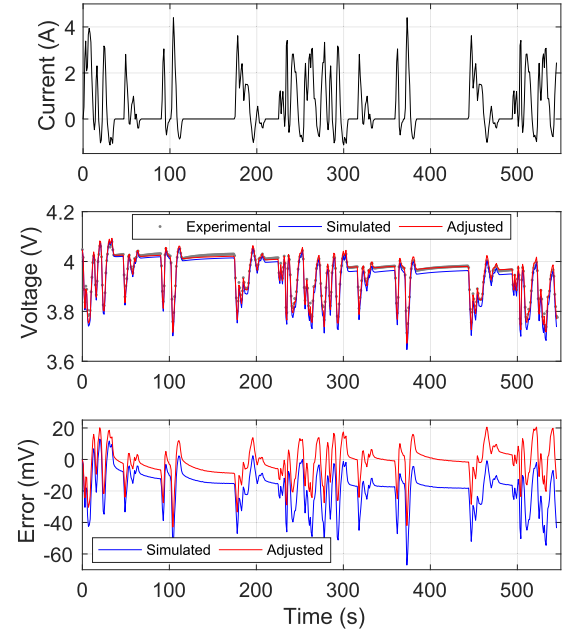

Fig. 9. Time domain comparison of SPM against measured data. Start point is 10% DoD and endpoint is 20% DoD.

OCV would require knowledge of Q_i^{th}. The time-domain linearized SPM was solved in MATLAB using Chebyshev orthogonal collocation as in our previous work [1], [45].

The comparison between linearized SPM and measured data is shown in Fig. 9 over a time period of almost 10 min. The DoD at the beginning of the period was 10% and at the end of the period was 20%. The OCV curves are almost linear over this range (see Fig. 5) and the variation in R_0 is small (Fig. 7). Initial results using this approach showed a consistent increasingly negative offset in voltage predictions over the time period examined. This is most likely due to the assumed OCV slope at this DoD being inaccurate, and was adjusted by multiplying the linearized cathode OCV slope by a factor of 0.78. Fig. 9 shows both the initial simulated and the adjusted simulated data in comparison to the measured data. The voltage errors between adjusted simulated versus measured data are max 20 mV and rms 10 mV. These are satisfyingly reasonable given the fact the model was parametrized completely separately with frequency-domain data that different cells were used for OCV measurements compared to EIS and time domain data, and that the kinetics were linearized despite current peaks of up to 6*C*.

VI. CONCLUSION

The analysis of parameter identifiability from experimental data is crucial prior to any attempt at estimating the parameters of battery first-principle models. We have demonstrated that the lithium-ion battery SPM is over-parametrized and that only six subgroups of parameters are necessary for full parametrization. Assuming that the OCV versus discharge capacity curves for each electrode are known, we have shown that the estimation of the linearized model parameters at a given DoD can only identify three parameters among these

six subgroups of parameters, namely, the cathode diffusion time constant τ_+^d, the anode diffusion time constant τ_-^d, and a charge-transfer resistance R_{ct}. Finally, we have shown the crucial role of the slope of electrode OCV curves on the parameter uncertainty. This has been investigated through analysis of the model, as well as through fitting both time and frequency-domain data. A flat electrode OCV curve results in high uncertainties on the electrode diffusion parameter. Therefore, impedance data at a single DoD cannot, in general, result in accurate parameter estimation for both electrodes, and experimental data at multiple DoDs must be considered. Specifically, complimentary DoDs where in turn the anode and cathode OCV gradients are significant must be chosen to yield satisfactory identifiability. Future work could investigate the effects of temperature on parameter estimation, and the evolution of cell parameters as a battery ages.

Acknowledgment

References

[1] A. M. Bizeray, S. Zhao, S. R. Duncan, and D. A. Howey, "Lithium-ion battery thermal-electrochemical model-based state estimation using orthogonal collocation and a modified extended Kalman filter," *J. Power Sources*, vol. 296, pp. 400–412, Nov. 2015.

[2] R. Klein, N. A. Chaturvedi, J. Christensen, J. Ahmed, R. Findeisen, and A. Kojic, "State estimation of a reduced electrochemical model of a lithium-ion battery," in *Proc. Amer. Control Conf. (ACC)*, Baltimore, MD, USA, Jul. 2010, pp. 6618–6623.

[3] S. J. Moura, N. A. Chaturvedi, and M. Krstić, "Constraint management in Li-ion batteries: A modified reference governor approach," in *Proc. Amer. Control Conf. (ACC)*, Washington, DC, USA, Jun. 2013, pp. 5332–5337.

[4] H. Perez, N. Shahmohammadhamedani, and S. Moura, "Enhanced performance of li-ion batteries via modified reference governors and electrochemical models," *IEEE/ASME Trans. Mechatron.*, vol. 20, no. 4, pp. 1511–1520, Aug. 2014.

[5] N. A. Chaturvedi, R. Klein, J. Christensen, J. Ahmed, and A. Kojic, "Algorithms for advanced battery-management systems," *IEEE Control Syst.*, vol. 30, no. 3, pp. 49–68, Jun. 2010.

[6] S. J. Moura and H. Perez, "Better batteries through electrochemistry," *Mech. Eng.*, vol. 136, no. 6, pp. S15–S21, 2014.

[7] S. Santhanagopalan and R. E. White, "Online estimation of the state of charge of a lithium ion cell," *J. Power Sources*, vol. 161, no. 2, pp. 1346–1355, Oct. 2006.

[8] K. A. Smith, C. D. Rahn, and C.-Y. Wang, "Model-based electrochemical estimation of lithium-ion batteries," in *Proc. IEEE Int. Conf. Control Appl.*, San Antonio, TX, USA, Sep. 2008, pp. 714–719.

[9] D. Di Domenico, A. Stefanopoulou, and G. Fiengo, "Lithium-ion battery state of charge and critical surface charge estimation using an electrochemical model-based extended Kalman filter," *J. Dyn. Syst., Meas., Control*, vol. 132, no. 6, p. 061302, 2010.

[10] K. A. Smith, C. D. Rahn, and C.-Y. Wang, "Model-based electrochemical estimation and constraint management for pulse operation of lithium ion batteries," *IEEE Trans. Control Syst. Technol.*, vol. 18, no. 3, pp. 654–663, May 2010.

[11] S. J. Moura, N. A. Chaturvedi, and M. Krstić, "Adaptive partial differential equation observer for battery state-of-charge/state-of-health estimation via an electrochemical model," *J. Dyn. Syst. Meas. Control*, vol. 136, no. 1, p. 011015, 2014.

[12] K. D. Stetzel, L. L. Aldrich, M. S. Trimboli, and G. L. Plett, "Electrochemical state and internal variables estimation using a reduced-order physics-based model of a lithium-ion cell and an extended Kalman filter," *J. Power Sources*, vol. 278, pp. 490–505, Mar. 2015.

[13] S. Zhao, A. M. Bizeray, S. R. Duncan, and D. A. Howey, "Performance evaluation of an extended Kalman filter for state estimation of a pseudo-2D thermal-electrochemical lithium-ion battery model," in *Proc. ASME Dyn. Syst. Control Conf.*, Columbus, OH, USA, 2015, pp. 1–5.

[14] P. W. C. Northrop, V. Ramadesigan, S. De, and V. R. Subramanian, "Coordinate transformation, orthogonal collocation, model reformulation and simulation of electrochemical-thermal behavior of lithium-ion battery stacks," *J. Electrochem. Soc.*, vol. 158, no. 12, pp. A1461–A1477, 2011.

[15] A. P. Schmidt, M. Bitzer, Á. W. Imre, and L. Guzzella, "Experiment-driven electrochemical modeling and systematic parameterization for a lithium-ion battery cell," *J. Power Sources*, vol. 195, no. 15, pp. 5071–5080, 2010.

[16] V. Ramadesigan, K. Chen, N. A. Burns, V. Boovaragavan, R. D. Braatz, and V. R. Subramanian, "Parameter estimation and capacity fade analysis of lithium-ion batteries using reformulated models," *J. Electrochem. Soc.*, vol. 158, no. 9, pp. A1048–A1054, 2011.

[17] J. C. Forman, S. J. Moura, J. L. Stein, and H. K. Fathy, "Genetic parameter identification of the Doyle-Fuller-Newman model from experimental cycling of a LiFePO$_4$ battery," in *Proc. Amer. Control Conf. (ACC)*, San Francisco, CA, USA, Jul. 2011, pp. 362–369.

[18] J. C. Forman, S. J. Moura, J. L. Stein, and H. K. Fathy, "Genetic identification and fisher identifiability analysis of the Doyle-Fuller-Newman model from experimental cycling of a LiFePO$_4$ cell," *J. Power Sources*, vol. 210, pp. 263–275, Jul. 2012.

[19] J. Marcicki, M. Canova, A. T. Conlisk, and G. Rizzoni, "Design and parametrization analysis of a reduced-order electrochemical model of graphite/LiFePO$_4$ cells for SOC/SOH estimation," *J. Power Sources*, vol. 237, pp. 310–324, Sep. 2013.

[20] S. Jiang, "A parameter identification method for a battery equivalent circuit model," SAE Tech. Paper 2011-01-1367, 2011, pp. 1–9.

[21] R. Al-Nazer, V. Cattin, P. Granjon, and M. Montaru, "A new optimization algorithm for a li-ion battery equivalent electrical circuit identification," in *Proc. 9th Int. Conf. Modeling, Optim. Simulation (MOSIM)*, Bordeaux, France, 2012, pp. 1–7.

[22] J. Jang and J. Yoo, "Equivalent circuit evaluation method of lithium polymer battery using bode plot and numerical analysis," *IEEE Trans. Energy Convers.*, vol. 26, no. 1, pp. 290–298, Mar. 2011.

[23] N. Moubayed, J. Kouta, A. El-Ali, H. Dernayka, and R. Outbib, "Parameter identification of the lead-acid battery model," in *Proc. 33rd IEEE Photovoltaic Spec. Conf.*, May 2008, pp. 1–6.

[24] M. Doyle, T. F. Fuller, and J. Newman, "Modeling of galvanostatic charge and discharge of the lithium/polymer/insertion cell," *J. Electrochem. Soc.*, vol. 140, no. 6, pp. 1526–1533, 1993.

[25] S. Atlung, K. West, and T. Jacobsen, "Dynamic aspects of solid solution cathodes for electrochemical power sources," *J. Electrochem. Soc.*, vol. 126, no. 8, pp. 1311–1321, 1979.

[26] G. Ning and B. N. Popov, "Cycle life modeling of lithium-ion batteries," *J. Electrochem. Soc.*, vol. 151, no. 10, pp. A1584–A1591, 2004.

[27] E. Barsoukov and J. R. Macdonald, *Impedance Spectroscopy: Theory, Experiment, and Applications*. Hoboken, NJ, USA: Wiley, 2005, p. 595.

[28] S. Tippmann, D. Walper, L. Balboa, B. Spier, and W. G. Bessler, "Low-temperature charging of lithium-ion cells part I: Electrochemical modeling and experimental investigation of degradation behavior," *J. Power Sources*, vol. 252, pp. 305–316, Apr. 2014.

[29] M. D. Murbach, V. W. Hu, and D. T. Schwartz, "The impedance analyzer: An open-source, Web-based tool for sophisticated interrogation of experimental EIS spectra," in *Proc. ECS Meeting Abstr.*, 2017, p. 320.

[30] S. Santhanagopalan, Q. Guo, and R. E. White, "Parameter estimation and model discrimination for a lithium-ion cell," *J. Electrochem. Soc.*, vol. 154, no. 3, pp. A198–A206, 2007.

[31] R. Bellman and K. J. Åström, "On structural identifiability," *Math. Biosci.*, vol. 7, pp. 329–339, Apr. 1970.

[32] L. Ljung, *System Identification: Theory for the User*. Englewood Cliffs, NJ, USA: Prentice-Hall, 1999.

[33] S. S. M. Alavi, A. Mahdi, S. J. Payne, and D. A. Howey. (2016). "Identifiability of generalised Randles circuit models." [Online]. Available: https://arxiv.org/abs/1505.00153

[34] C. R. Birkl, E. McTurk, M. R. Roberts, P. G. Bruce, and D. A. Howey, "A parametric open circuit voltage model for lithium ion batteries," *J. Electrochem. Soc.*, vol. 162, no. 12, pp. A2271–A2280, 2015.

[35] E. McTurk, C. R. Birkl, M. R. Roberts, D. A. Howey, and P. G. Bruce, "Minimally invasive insertion of reference electrodes into commercial lithium-ion pouch cells," *ECS Electrochem. Lett.*, vol. 4, no. 12, pp. A145–A147, 2015.

[36] B. S. Haran, B. N. Popov, and R. E. White, "Determination of the hydrogen diffusion coefficient in metal hydrides by impedance spectroscopy," *J. Power Sources*, vol. 75, pp. 56–63, Sep. 1998.

[37] Q. Guo, V. R. Subramanian, J. W. Weidner, and R. E. White, "Estimation of diffusion coefficient of lithium in carbon using AC impedance technique," *J. Electrochem. Soc.*, vol. 149, no. 3, pp. A307–A318, 2002.

[38] G. Sikha and R. E. White, "Analytical expression for the impedance response of an insertion electrode cell," *J. Electrochem. Soc.*, vol. 154, no. 1, pp. A43–A54, 2007.

[39] S. Buller, M. Thele, E. Karden, and R. W. De Doncker, "Impedance-based non-linear dynamic battery modeling for automotive applications," *J. Power Sources*, vol. 113, no. 2, pp. 422–430, 2003.

[40] D. A. Howey, P. D. Mitcheson, V. Yufit, G. J. Offer, and N. P. Brandon, "Online measurement of battery impedance using motor controller excitation," *IEEE Trans. Veh. Technol.*, vol. 63, no. 6, pp. 2557–2566, Jun. 2014.

[41] M. Ecker, T. K. D. Tran, P. Dechent, S. Käbitz, A. Warnecke, and D. U. Sauer, "Parameterization of a physico-chemical model of a lithium-ion battery I. Determination of parameters," *J. Electrochem. Soc.*, vol. 162, no. 9, pp. A1836–A1848, 2015.

[42] T. F. Fuller, M. Doyle, and J. Newman, "Simulation and optimization of the dual lithium ion insertion cell," *J. Electrochem. Soc.*, vol. 141, no. 1, pp. 1–10, 1994.

[43] M. Guo, G. Sikha, and R. E. White, "Single-particle model for a lithium-ion cell: Thermal behavior," *J. Electrochem. Soc.*, vol. 158, no. 2, pp. A122–A132, 2011.

[44] S. Zhao, S. R. Duncan, and D. A. Howey, "Observability analysis and state estimation of lithium-ion batteries in the presence of sensor biases," *IEEE Trans. Control Syst. Technol.*, vol. 25, no. 1, pp. 326–333, Jan. 2017.

[45] A. M. Bizeray, J. Reniers, and D. A. Howey. (2016). *Spectral_Li-Ion_SPM: Initial Release*, doi. http://doi.org/10.5281/zenodo.212178.

Jin–Ho Kim, photograph and biography not available at the time of publication.

Stephen R. Duncan (M'96) received the M.A. degree in physics from the University of Cambridge, Cambridge, U.K., and the M.Sc. and Ph.D. degrees in control systems from the Imperial College London, London, U.K.

From 1993 to 1998, he was a Reader with the Control Systems Centre, University of Manchester, Manchester, U.K., and the Director of the Greycon Limited (a spin-out company from Imperial College London), London. He is currently a Professor with the Department of Engineering Science, University of Oxford, Oxford, U.K., where he is a member of the Control Group.

Dr. Duncan is a Fellow of the St Hugh's College, Oxford, and a member of the Editorial Board of the *IET Proceedings Control Theory and Applications*.

Adrien M. Bizeray received the French Engineering Diploma from the Arts et Métiers ParisTech, Angers, France, the M.Sc. degree in advanced mechanical engineering from the Imperial College London, London, U.K., and the D.Phil. degree from the University of Oxford, Oxford, U.K., in 2017.

His current research interests include the mathematical modeling of lithium-ion batteries for developing the next-generation of battery-management systems relying on electrochemical model-based state estimation and control algorithms for improved battery safety and lifetime.

David A. Howey (M'10–SM'17) received the B.A. and M.Eng. degrees from Cambridge University, Cambridge, U.K., in 2002, and the Ph.D. degree from the Imperial College London, London, U.K., in 2010.

He is currently an Associate Professor with the Department of Engineering Science, Energy and Power Group, University of Oxford, Oxford, U.K. He was involved in projects on battery degradation diagnostics and prognostics, battery modeling, optimal control of charging and discharging, energy storage and microgrids, thermal management, novel pack designs, and motor degradation. His current research interests include condition monitoring and management of electric and hybrid vehicle components.